Original Article

# Structural and Optical Properties Study of SnS: Ag Doped Cu Thin Films Prepared by PLD Technique for Solar Cell Application

**Ameira A. Almaula[1], Çiğdem Yüksektepe Ataol[2], Ghuson H. Mohammed[3]**

[1,2]Çankırı Karatekin University, Faculty of Science, Department of Physics, 18100, Çankırı, Turkey

[3]University of Baghdad, Collage of Science, Department of Physics, Baghdad, Iraq

## Abstract

Cu-doped SnS: Ag thin films have been fabricated by the PLD technique to modify specific properties of SnS films for a promising approach to reduce the anti site defects and further improve the efficiency of choosing the optimum condition to fabricated SnS: Ag solar cell by oping with different ratios of Cu deposited on Si wafers. A significant effect of the Cu doping ratio is noticed on the XRD pattern and optical properties of prepared thin films.The results of XRD show the polycrystalline nature of the prepared SnS powder and broad lines for thin films as its nanocrystalline structure. Additional phases appeared corresponding to Ag and Cu at a high ratio. The crystallite size reduced from 15.4 to12.8 nm after doping with 0.05 Cu and increased up to 14.7 with an increasing Cu ratio to 0.15 while the lattice strain has the opposite behavior. The optical absorbance increases for the SnS: Ag sample and more increasing with the Cu content. A red shift in the band edge with Cu doping appeared. The band gap reduced from 2.2 eV for SnS to 1.75 eV for (SnS:Ag)0.85Cu0.15.

**Keywords:** Structural and optical properties, Ag doped SnS, thin films, XRD technique, PLD technique, FT-IR, optical properties, solar cell.

## 1. Introduction

Scientists and researchers have been studying semiconductors since the early 19th century, which possess unique electrical and optical properties that make them the basic structure of modern electronic technologies. Semiconductors have a high impedance to the passage of electric current at low temperatures, while their electrical conductivity increases significantly at high temperatures [1].

Thin-film science is an important area of modern technology. The term thin film is used to describe one or more layers of atoms of a substance that are less than one micron thick. Because the film layer is thin, it is deposited on various materials known as substrates, including glass, silicon, and metal. The use of thin films is critical in a variety of industries and research in solar cells and other photovoltaic applications [2].

Tin sulfide is of interest substance for use in thin film solar cells application. This is because of the abundant and non-toxicity of its component elements, tin, and sulfur. Tin sulfide direct energy band gap has an optimal value for photovoltaic application to harvest optimum energy from solar radiation [3].

Recently, the focus of advanced materials studies has been on the creation of particles with regulated size and shape using a straightforward and affordable process, which is technologically crucial for the important issues being addressed by contemporary material science [4].

**Address for correspondence: Ameira A. Almaula**
Çankırı Karatekin University, Faculty of Science, Department of Physics, 18100, Çankırı, Turkey
Email: amira_almaula@yahoo.com



How to cite this article: Ameira A. Almaula, Çiğdem Yüksektepe Ataol, Ghuson H. Mohammed, Structural and Optical Properties Study of SnS: Ag Doped Cu Thin Films Prepared by PLD Technique for Solar Cell Application, J PHARM NEGATIVE RESULTS 2022;13: 936-944.

**Access this article online**

**Quick Response Code:**

**Website:** www.pnrjournal.com

**DOI:** 10.47750/pnr.2022.13.04.127

The Pulse laser technique is a simple technique can be controlled to the deposited films properties. PLD method is an appropriate technique for the prepared of composite semiconductors which have high melting and evaporation temperatures. It is assumed a bottom-up method which includes the construction of the deposited matter from the sputtered atoms or molecules [5].

Though, many previous studies were concerned with improving the conversion efficiency for photovoltaic, still, more studies are needed for investigation of alternative low cost materials for solar cell application sing simple low cost technique. In this work, we try to improve the SnS/Si heterojunction efficiency by compose with silver and copper ions as dopant by studying of structural, surface morphology, optical properties, and electrical properties of the pure and doped SnS thin films.

## 2. Experimental

Tin SulphideSnxS1-x was prepared by solid-state reaction route under vacuum. The same atomic ratio of (99.999%) purity (Sn and S) elements according to their atomic percentages (Sn:S = 0.5:0.5) were used. The mixed elements were sealed in an evacuated (~10-3 Torr) quartz ampoule and heated to 1200 °C for 5 hours, according to the face diagram of Sn-S, then cooled to room temperature. The prepared SnS was mixed with silver Ag (of 9% atm percentage) from Nanjing Nano Technology Co. ltd with a purity of 99.99% and Copper Cu from Chem-Lab NV with the purity of 99.5% were mixed at different concentration of x= (0.05, 0.1, and 0.15) wt. %. The powder of precursors was mixed using a gate mortar for one hour. It was pressed into pellets of 1cm diameter and 0.2 cm thickness, using a hydraulic press type (SPECAC), under press of 6 tons for 10 minutes.

Glass slides (1.25×1) cm2 area were used as substrates for deposition, to study the structural and optical properties of (SnS,SnS:Ag,SnS:Ag:Cu) thin films, because its low cost and the results were not affected by the amorphous structure.

Also n-type and p-type Si wafers(opposite type than the deposited material type) with crystal orientation (100) was used as a substrate for the construction of the photovoltaic devices of (SnS, SnS:Ag, and doped SnS:Ag at different Cu ratios).

The (SnS,SnS:Ag, and SnS:Ag:Cu ) thin films were produced by the Nd:YAG laser (Huafei Tonged Technology—DIAMOND-288 pattern EPLS). The PLD procedure was carried out inside a vacuum around (10-2 mbar). The focused Nd:YAG laser beam of 800 mJ at 1064 nm wavelength, pulse width 10 ns, and repetition frequency6 Hz, for 300 laser pulses incident on the target surface at incident angle of 45° with the target surface. The distance between the target and the laser was set at the focal length of the laser (10 cm).

The thin film thicknesses were measured according to the principle of reflectance from thin films using an optical bench kit. He-Ne laser of 632 nm wavelength. The interference pattern is used to determine the film thickness (t) according to the relation:

$$t = \frac{\lambda}{2}\frac{\Delta x}{x} \quad \text{(2.1)}$$

where λ is the used laser wavelength, x is the width of bright fringes, Δx is the thickness of dark fringes.

2.1 Structural Property Measurements

The crystal structure of (SnS, SnS:Ag, and SnS:Ag:Cu) thin films was examined by X-ray diffraction technique.X-ray diffraction device (LabX XRD-8000), was used with specifications(Source = Cu-K, Current = 30 mA, voltage = 40 kV, wavelength = 1.5406 Å, range of diffraction angle = 20-80°, scanning speed = 5 degree/min)

When a beam of X-rays is fall at a certain angle on the surface of a crystalline sample as a result of Bragg's reflections from the parallel crystal surfaces a diffraction pattern was formed. When amorphous thin film was tested, the reflected pattern does not form any peaks, meaning that the interference of the reflected beams is destructive. But when the thin film is arranged in a crystalline feature, the interference is constructive, due to the reflection from regular crystals without any scattering by the beams reflected from those crystal surfaces as a result of their regularity. Thus, peaks appear indicating the constructive interference of the X-ray waves reflected from parallel crystal surfaces as a result of the fulfillment of Bragg's condition [6].

$$n\,\lambda = 2\,d_{hkl}\,\sin\theta \quad \text{(2.2)}$$

Where n is the diffraction order, is the wavelength of the incident rays, dhkl is the distance between two successive planes,h, k, l represents the miller indicesand θ is the angle of incidence and reflection of an X-ray beam falling on a given surface. When knowing the angles corresponding to these peaks, the dhklvalueis determined through Bragg's law and fromdhkl value the Miller's coefficients (hkl) are determined according to the standard card, and through those coefficients, the crystalline structure is determined.

The relation between the crystallite size (C.S) and the full width at half maximum (FWHM) of diffraction lines was determined by the Debye-Scherer formula [7]:

$$C.S = \frac{0.9\,\lambda}{FWHM\,.cos(\theta)} \quad \text{(2.3)}$$

While, the uniform strain of an induced lattice by defects or Nano-size effect, is determined according to the relation [8]:

$$\varepsilon = \frac{\beta\,\mathrm{Cos}\theta}{4} \quad \text{(2.4)}$$

### 2.2 Optical Property Measurements

The optical properties of the synthesized nanocomposite films deposited on glass substrates were examined. The UV-visible transmittance spectroscopy was used to study the optical properties of the thin films of SnS, SnS:Ag, and SnS:Ag:Cu at different ratios of Cu(0.05,0.10, and 0.15) deposited on glass slides.A two-beam UV-vis spectrophotometer (UV-1800 Shimadzu was used at the spectral region (300-1100 nm). The sample on which the film is deposited is placed well in the base window so that the light rays fall perpendicular to the thin film. A glass slide similar to the used glass substrates is used as a reference to cancel out the effect of the glass and record only the film transparency. The collected data in computer are used to calculate the optical absorbance, absorption coefficient, energy band gap.

## 3. Results And Discussion

### 3.1 X-ray Diffraction Results

Figure 3.1 shows the XRD pattern for the used SnS powder,prepared by solid-state reaction routeunder vacuum,compared to the standard diffraction lines card no. (96-810-4282). The polycrystalline structure of pure orthorhombic SnS phase identical with the standard lines has appeared.

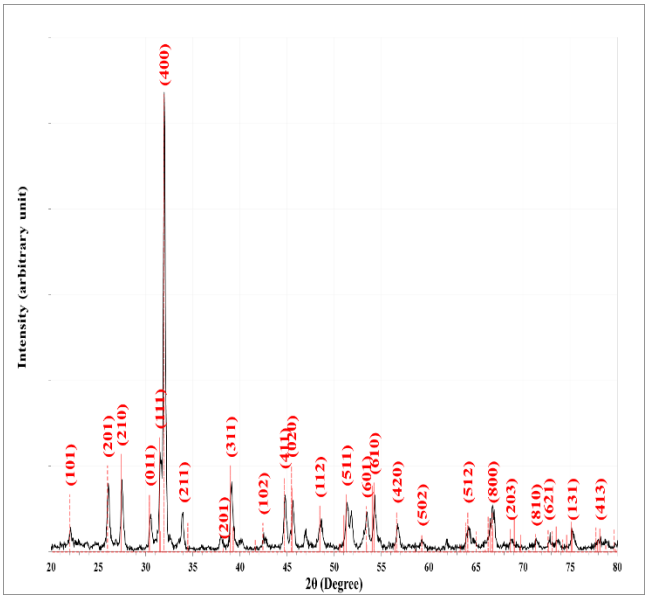


Figure3.1 XRD pattern for SnS powder.

The intermolecular plans spacing (dhkl) was determined using Braggs formula (equation 2.2), while the crystallite size (C.S) was determined according to Debye-Scherrer's formula using the full width at half maxima for the diffraction lines (equation 2.3) while the lattice strain induced after the doping process was determined using equation 2.4. Table 3.1 illustrate the XRD parameters for the diffraction peaks. The average crystalline size was 23.8 nm.

Table 3.1 XRD parameters (2θ, FWHM, dhkl, C.S, hkl) for the SnS pellet.

| 2θ (Deg.) | FWHM (Deg.) | $d_{hkl}$ Exp.(Å) | C.S (nm) | hkl |
|---|---|---|---|---|
| 22.0357 | 0.3000 | 4.0306 | 27.0 | (101) |
| 26.0857 | 0.3215 | 3.4132 | 25.4 | (201) |
| 27.5000 | 0.3429 | 3.2408 | 23.9 | (210) |
| 30.5857 | 0.3429 | 2.9205 | 24.0 | (011) |
| 31.5714 | 0.3214 | 2.8316 | 25.7 | (111) |
| 32.0000 | 0.2786 | 2.7946 | 29.7 | (400) |
| 33.9500 | 0.3214 | 2.6384 | 25.8 | (211) |
| 37.9786 | 0.3857 | 2.3673 | 21.8 | (201) |
| 39.1357 | 0.3643 | 2.2999 | 23.1 | (311) |
| 42.6071 | 0.4929 | 2.1202 | 17.3 | (102) |
| 44.8143 | 0.3643 | 2.0208 | 23.6 | (411) |
| 45.6286 | 0.3858 | 1.9866 | 22.3 | (200) |
| 48.5643 | 0.4929 | 1.8732 | 17.7 | (112) |
| 51.3929 | 0.4072 | 1.7765 | 21.7 | (511) |
| 53.4071 | 0.3214 | 1.7142 | 27.7 | (601) |
| 54.2857 | 0.3643 | 1.6885 | 24.5 | (610) |
| 56.7071 | 0.3643 | 1.6220 | 24.8 | (420) |
| 59.3429 | 0.3857 | 1.5561 | 23.7 | (502) |
| 64.2286 | 0.4500 | 1.4490 | 20.8 | (512) |
| 66.7571 | 0.5786 | 1.4001 | 16.4 | (800) |
| 68.7500 | 0.3429 | 1.3643 | 28.1 | (203) |

| | | | | |
|---|---|---|---|---|
| 71.4286 | 0.3643 | 1.3196 | 26.9 | (810) |
| 72.8000 | 0.3858 | 1.2981 | 25.6 | (621) |
| 75.2000 | 0.4286 | 1.2625 | 23.4 | (131) |

Figure 3.2 shows the XRD patterns for the prepared thin films by PLD technique of SnS, and SnS:Ag at different Cu ratios compared with the standard diffraction lines of the standard card no. 96-810-4282. Polycrystalline structure of low crystallinity for all samples was appeared. All peaks appeared as broad feature indicate on nanocrystalline structure. For the SnS thin films the diffraction lines located at diffraction angles (2θ) 25.9113°, 27.5158°, 31.8790°, 39.0007°, and 45.4750° corresponding to the crystalline planes (201), (210), (400), (311), and (020) for the orthorhombicSnS structure. These diffraction lines were slightly shifted after composing with silver due to strain in the lattice as a result of the incorporation of strange ions within the host lattice, or due to variation of crystallite size. Additional diffraction lines at 2θ= 38.1844° and 44.2083° appeared corresponding to crystal planes of (111), and (200) for cubic Ag, respectively, according to the standard card (96-901-2432).

Small variation in the diffraction pattern after doping with 0.05 Cu. While Additional peak for the diffraction plane (111) corresponding to the copper structure is located at 43.5327° according to standard card no. (96-500-0217) appeared for samples doped with a higher ratio. The appearance of the new phase at high doping concentration indicates that the added ratio exceeds the solubility limit of the host matrix. The addition of a small number of dopant impurities leads to a solid solution of the dopants; increasing the doping concentration beyond the low solubility limit leads to supersaturated solutions in the host lattice, so appeared as a separate phase [9].

The line breadth varies according to the Cu ratio indicating that this ratio affects the growth of nanoparticles due to the difference in nanoparticle's growth. Table 3.2 illustrate the XRD parameters for the diffraction peaks. The result patterns agree with the previous study [10].

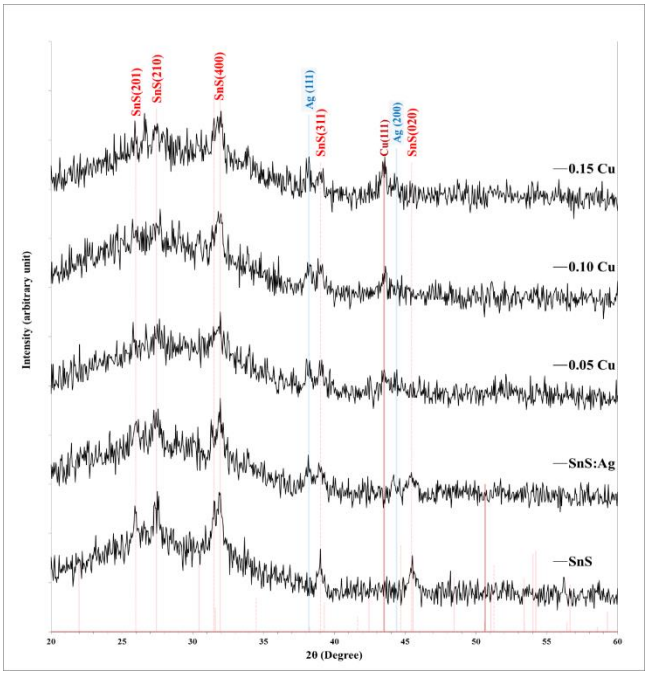


Figure 3.2 XRD patterns of the thin films prepared by PLD technique for SnS, SnS:Ag, and Cu-doped SnS:Ag at different ratios.

Table 3.2 XRD parameters for the thin films prepared by PLD for SnS, SnS:Ag, and Cu-doped SnS:Ag at different ratios.

| Sample | 2θ (Deg.) | FWHM (Deg.) | $d_{hkl}$ Exp.(Å) | C.S (nm) | hkl | Phase | Lattice strain |
|---|---|---|---|---|---|---|---|
| SnS | 25.9113 | 0.3096 | 3.4358 | 26.3 | (201) | Orth. SnS | 0.0013 |
| | 27.5158 | 0.4504 | 3.2390 | 18.2 | (210) | Orth. SnS | 0.0019 |
| | 31.8790 | 0.4504 | 2.8049 | 18.3 | (400) | Orth. SnS | 0.0019 |
| | 39.0007 | 0.5348 | 2.3076 | 15.8 | (311) | Orth. SnS | 0.0022 |
| | 45.4750 | 0.5348 | 1.9930 | 16.1 | (020) | Orth. SnS | 0.0022 |
| SnS:Ag | 25.9958 | 0.4786 | 3.4248 | 17.0 | (201) | Orth. SnS | 0.0020 |
| | 27.4032 | 0.6475 | 3.2521 | 12.6 | (210) | Orth. SnS | 0.0027 |
| | 31.9071 | 0.5348 | 2.8025 | 15.4 | (400) | Orth. SnS | 0.0022 |
| | 38.1844 | 0.5630 | 2.3550 | 14.9 | (111) | Cub. Ag | 0.0023 |
| | 38.9726 | 0.5348 | 2.3092 | 15.8 | (311) | Orth. SnS | 0.0022 |
| | 44.2083 | 0.4504 | 2.0471 | 19.0 | (200) | Cub. Ag | 0.0018 |

| | | | | | | | |
|---|---|---|---|---|---|---|---|
| | 45.4469 | 0.8163 | 1.9941 | 10.6 | (020) | Orth. SnS | 0.0033 |
| **0.05 Cu** | 27.6284 | 0.6756 | 3.2261 | 12.1 | (210) | Orth. SnS | 0.0029 |
| | 31.8508 | 0.6474 | 2.8074 | 12.8 | (400) | Orth. SnS | 0.0027 |
| | 38.1562 | 0.4786 | 2.3567 | 17.6 | (111) | Cub. Ag | 0.0020 |
| | 39.0852 | 0.3940 | 2.3028 | 21.4 | (311) | Orth. SnS | 0.0016 |
| | 43.5327 | 0.4786 | 2.0773 | 17.9 | (111) | Cub. Cu | 0.0019 |
| **0.10 Cu** | 27.4314 | 0.6474 | 3.2488 | 12.6 | (210) | Orth. SnS | 0.0027 |
| | 31.9071 | 0.5912 | 2.8025 | 14.0 | (400) | Orth. SnS | 0.0025 |
| | 38.2970 | 0.6193 | 2.3483 | 13.6 | (111) | Cub. Ag | 0.0026 |
| | 39.0007 | 0.5066 | 2.3076 | 16.6 | (311) | Orth. SnS | 0.0021 |
| | 43.5890 | 0.5067 | 2.0747 | 16.9 | (111) | Cub. Cu | 0.0021 |
| **0.15 Cu** | 25.9395 | 0.6474 | 3.4321 | 12.6 | (201) | Orth. SnS | 0.0028 |
| | 27.4877 | 0.5067 | 3.2423 | 16.1 | (210) | Orth. SnS | 0.0021 |
| | 31.8790 | 0.5630 | 2.8049 | 14.7 | (400) | Orth. SnS | 0.0024 |
| | 38.1562 | 0.5067 | 2.3567 | 16.6 | (111) | Cub. Ag | 0.0021 |
| | 39.0570 | 0.5348 | 2.3044 | 15.8 | (311) | Orth. SnS | 0.0022 |
| | 43.5327 | 0.5349 | 2.0773 | 16.0 | (111) | Cub. Cu | 0.0022 |
| | 44.3772 | 0.5911 | 2.0397 | 14.5 | (200) | Cub. Ag | 0.0024 |

Figure 3.3 shows the variation of crystallite size and lattice strain along the (400) direction of the SnS:Ag and Cu-doped SnS:Ag thin films prepared by the PLD technique with the Cu ratio. It seems that the crystallite size reduced from 15.4 to12.8 nm after doping with 0.05 Cu, then it increased to 14 and 14.7 with an increasing Cu ratio to 0.10 and 0.15, respectively. While the lattice strain has opposite behavior indicates that the main cause of lattice contraction is due to the nano-size effect as a result of the surface tension by the surface atoms in nanoparticles. This effect is very large at small sizes due to the increase in the area-to-volume ratio [11].

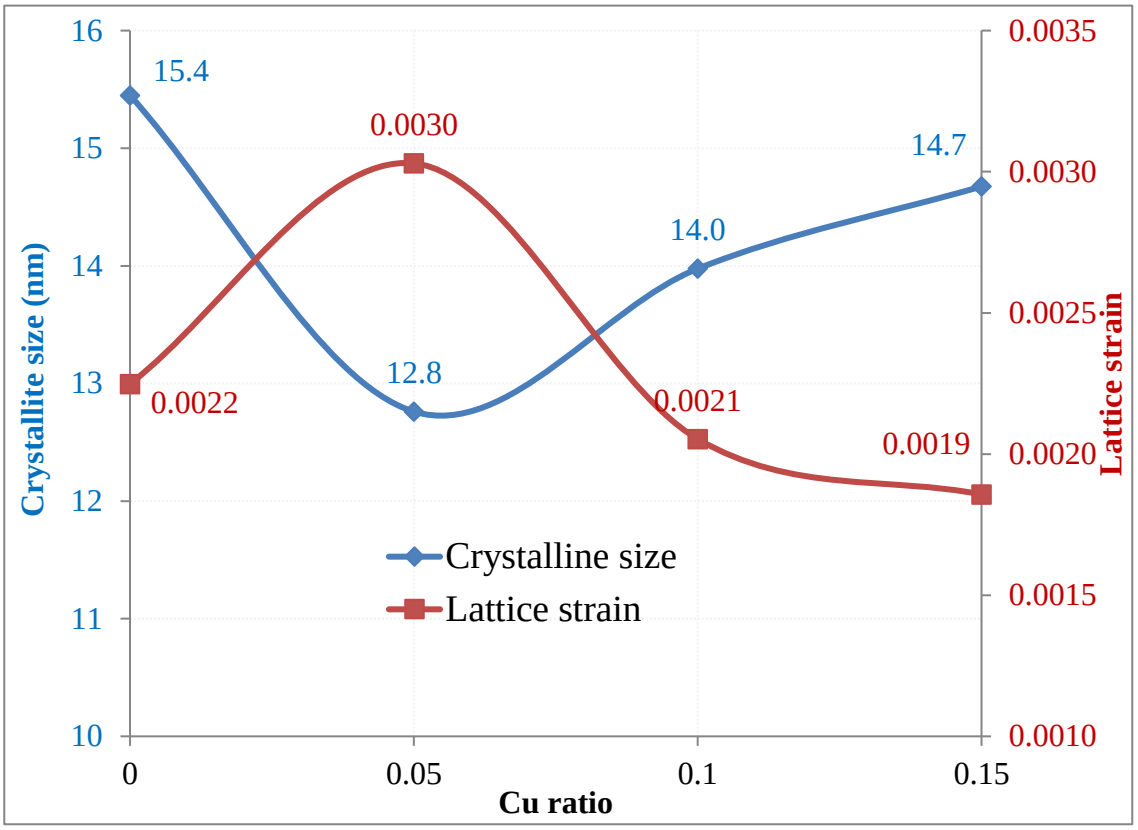


Figure 3.3 Variation of Crystallite size and lattice strain of the thin films prepared by PLD technique for Cu-doped SnS:Ag with the Cu ratio.

3.2 Furrier Transform Infrared Spectroscopy Results

To learn more about the potential structural components of the deposited thin films, FT-IR spectroscopy has been used. Figure 3.4 shows the Furrier transform infrared spectroscopy (FT-IR) patterns for the SnS, SnS:Ag, and Cu-doped SnS:Ag thin films deposited at different Cu ratios. Several well-defined absorption bands were observed in the spectra at about 3394.83, 2925.00, 2854.17, 2362.50, 2327.17, 1612.43, 1437.50, 1045.83, and 633.33 cm−1.

A broad band at 3394.83 cm−1 indicates stretching vibrations of O–H. The two bands at 2925.00 and 2854.17 cm−1 are assigned to the asymmetric and symmetric vibrations of CH2[12]. The double band located at 2362.50 and 2327.17 cm−1 is assigned to O=C=O vibrations in carbon dioxide [13]. The band at 1045.83cm−1 comes from the vibration of C–S [12]. The absorption bands located at 1437.50 and 633.33 cm−1 indicates the Sn-S bands [14]. Moreover, the appearance of the band at 1612.43 cm−1 correspond to C-O band [15]. The bands corresponding to strange atoms in the film probably come from the ambient.

As shown in Table 3.3, most bands shifted towards a higher wavenumber after doping with Ag, as well as an increase in the percentage of Cu doping indicates that Ag and Cu ions are successfully incorporated into the SnS matrix [16].

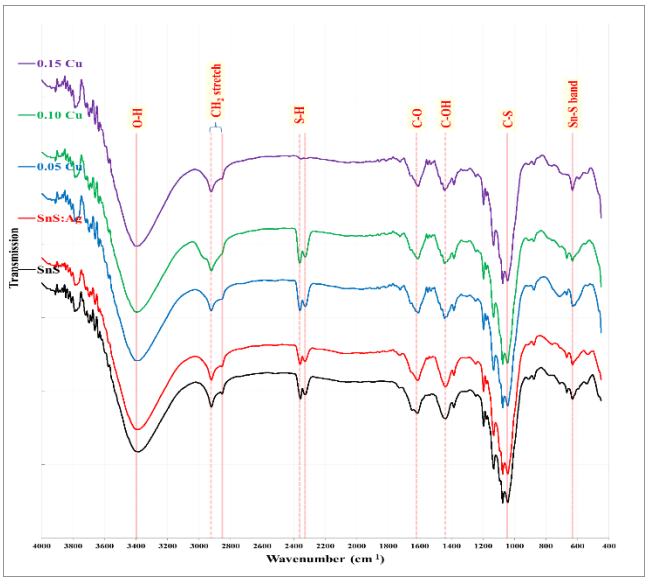


Figure 3.4 FT-IR patterns for the SnS, SnS:Ag and doped SnS:Ag at different Cu ratios.

Table 3.3 FT-IR bands for the thin films of SnS:Ag and Cu-doped SnS:Ag at different Cu ratios.

| Band Type | SnS | SnS:Ag | 0.05 Cu | 0.10 Cu | 0.15 Cu |
|---|---|---|---|---|---|
| **O-H stretch** | 3394.83 | 3395.22 | 3395.93 | 3404.17 | 3400.20 |
| **$CH_2$ Stretch** | 2925.00 | 2920.83 | 2923.66 | 2924.90 | 2925.00 |
| | 2854.17 | 2862.50 | 2870.83 | - | - |
| **S-H** | 2362.50 | 2363.40 | 2363.65 | 2363.77 | - |
| | 2327.17 | 2327.17 | 2328.22 | 2329.00 | - |
| **C-O** | 1612.43 | 1614.50 | 1615.60 | 1617.31 | 1618.20 |
| **C-OH** | 1437.50 | 1437.50 | 1441.67 | 1441.77 | 1445.83 |
| **C-S** | 1045.83 | 1041.67 | 1037.50 | 1041.67 | 1045.83 |
| **Sn-S** | 633.33 | 629.17 | 625.00 | 633.33 | 629.17 |

## 3.3 Optical Properties

### 3.3.1 UV-visible Absorbance

Figure 3.5 shows the absorbance curves for the deposited SnS, SnS:Ag, and Cu-doped SnS:Ag thin film samples at different Cu ratios. It appeared that the absorbance gradually decreased with wavelength indicated on low crystallinity for all samples, as shown by the XRD. Strong absorption at short wavelengths and low absorption at long wavelengths; only photons with enough energy can interact with semiconductors to produce electron-hole pairs [17]. It was observed that the absorbance increases for the SnS:Ag sample compared with the SnS sample, in addition, increasing the Cu content cause more increase in absorption due to creating localized levels within the energy bandgap, which acts as a springboard to promote the electronic transition. The red shift is the most obvious with Cu doping and significantly improves absorption in the visible range compared with other transition metals [18].

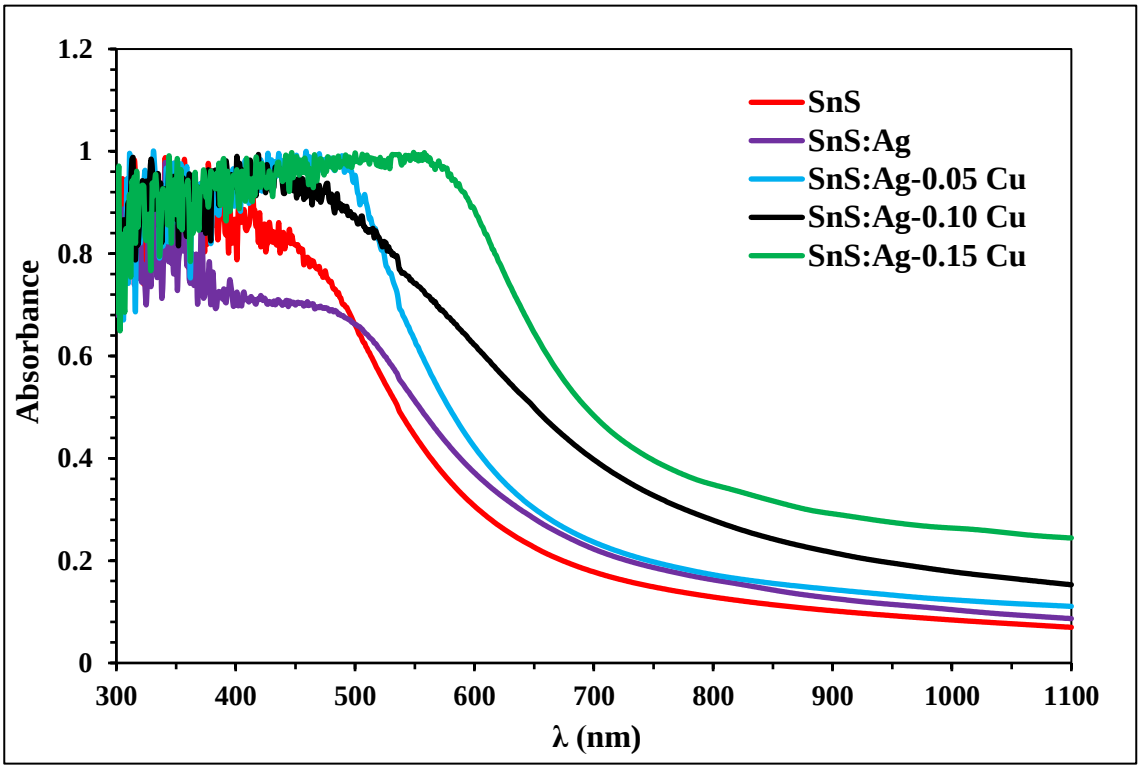


Figure 3.5 UV-visible absorbance spectra for the thin films of SnS, SnS:Ag, and Cu-doped SnS:Ag at different Cu ratios.

3.3.2 Absorption Coefficient

The absorption coefficient (α) for SnS, SnS:Ag, and Cu-doped SnS:Agthin film samples at different Cu ratios were determined. The variation of α with wavelength was shown in Figure 3.6. It has the same behavior as absorption spectra. The absorption coefficient in the range of 104, especially at low wavelengths indicate the direct electronic transition [19].

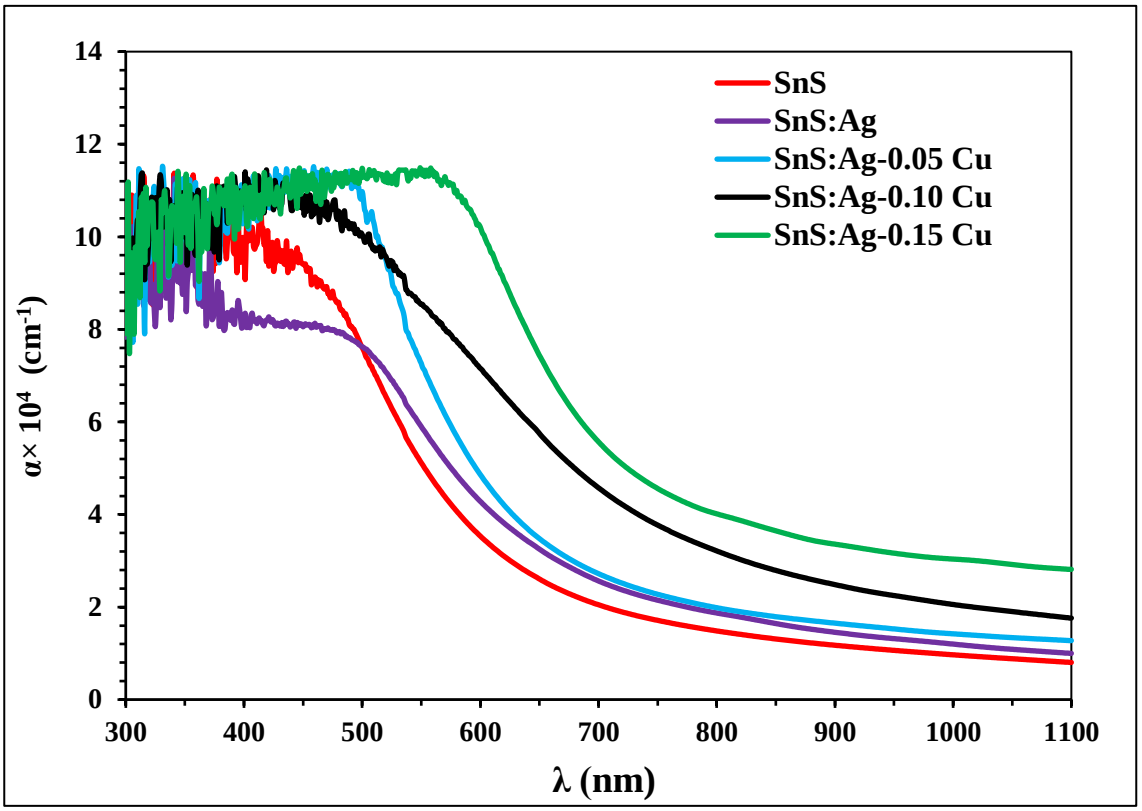


Figure 3.6 Absorption coefficient for the thin films prepared by PLD for Cu-doped SnS:Ag at different Cu ratios.

3.3.3 Optical Energy Gap

The optical energy bandgap (Egopt) for the SnS, SnS:Ag, and Cu-doped SnS:Ag thin films at different Cu ratios deposited by pulsed laser on glass slides were determined by using the Tauc formula as shown in Figure 3.7. This formula is used to determine the type of electronic transition by plotting the relations (αhυ)1/2, (αhυ)1/3,(αhυ)2/3,and (αhυ)2 against hvto find the best linear behavior. for all samples, the best linear relation was for (αhυ)2 which conformed to the allowed direct electronic transition behavior. The optical bandgap equals the cross point of the tangential line with the x-axis. The bandgap reduced from 2.2eV to 2.05 eV when the SnS sample composes with Ag. Doping the SnS:Ag sample with Cu cause more reduction of energy bandgap to 2.0, 1.8, and 1.75 eV at 0.05, 0.10, and 0.15 Cu ratios, respectively. The band gap values are close to the reported values[10]. The increase in the direct band gap compared to the bulk SnS (1-1.3 eV) are due to the quantum confinement effect[20]. Decreasing the band gap with increasing the metallic ions contents due to the creation of localized states near the valance and conductive bands [21]. Table 3.4 shows the optical energy band gap for the SnS, SnS:Ag, and Cu-doped SnS:Ag thin films prepared at different Cu ratios by PLD.

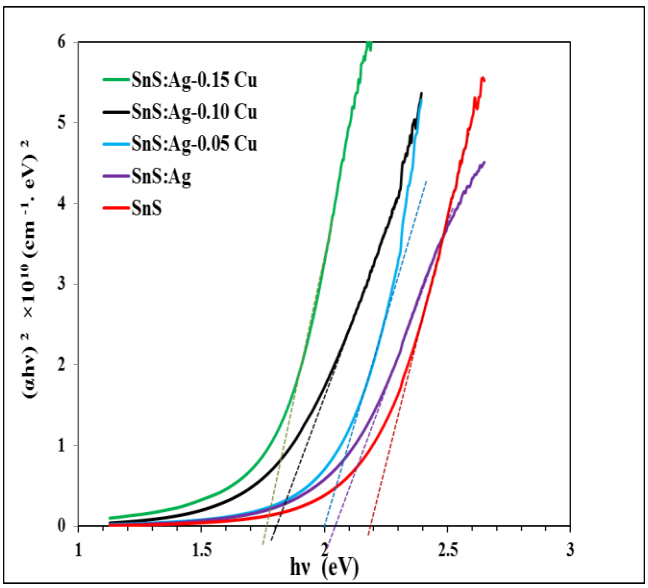


Figure 3.7 Calculation of energy gap for the SnS, SnS:Ag and Cu-doped SnS:Ag thin films prepared at different Cu ratios by PLD.

Table 3.4 Optical energy band gap E_g^(Opt.)for the SnS, SnS:Ag, and Cu-doped SnS:Ag thin films prepared at different Cu ratios by PLD.

| Sample | $E_g$ (eV) |
|---|---|
| **SnS** | 2.20 |
| **SnS:Ag** | 2.05 |
| **0.05 Cu** | 2.00 |
| **0.10 Cu** | 1.80 |
| **0.15 Cu** | 1.75 |

## 4. Conclusions

Study the characteristics of the SnS, SnS:Ag, Cu-doped SnS:Ag composites thin film at different Cu contents prepared by pulsed laser deposition technique show that it is possible to control the properties of the films prepared by doping at a specific ratio for use in a photovoltaic application.

The X-ray diffraction test shows the polycrystalline orthorhombic structure of broad lines feature indicates nanocrystalline for all samples. Additional phases corresponding to Ag and Cu at a high ratio appeared. The crystallite size for SnS:Ag thin films reduced from 15.4 to12.8 nm after doping with 0.05 Cu, then it increased to 14 and to 14.7 with an increasing Cu ratio to 0.10 and 0.15, respectively. While the lattice strain has opposite behavior indicates that the main cause of lattice contraction due to nano-size effect.

The FT-IR shows the characteristics bands for SnS in all samples in addition to the band of adsorbed gases from ambient. Most bands shifted towards a higher wavenumber after doping with Ag, as well as with Cu incorporated into the SnS matrix.

The absorbance curves at UV-visible appeared as a gradual absorption edge for all samples. The absorbance increases for the SnS:Ag sample compared with the SnS sample, in addition, increasing the Cu content cause more increase in absorption.

A redshift in band edge with Cu doping appeared

## References


1. Solymar, L., Walsh, D., & Syms, R. R. A. (2018). Semiconductors (Vol. 1). Oxford University Press. https://doi.org/10.1093/oso/9780198829942.003.0008.
2. Oluwatosin Abegunde, O., Titilayo Akinlabi, E., Philip Oladijo, O., Akinlabi, S., & Uchenna Ude, A. (2019). Overview of thin film deposition techniques. AIMS Materials Science, 6(2), 174–199. https://doi.org/10.3934/matersci.2019.2.174
3. Leach, M., Reddy, K. T. R., Reddy, M. V., Tan, J. K., Jang, D. Y., & Miles, R. W. (2012). Tin sulphide thin films synthesised using a two step process. In Energy Procedia (Vol. 15, pp. 371–378). https://doi.org/10.1016/j.egypro.2012.02.045
4. Vikraman, D., Thiagarajan, S., Karuppasamy, K., Sanmugam, A., Choi, J.-H., Prasanna, K., Maiyalagan, T., Thaiyan, M., & Kim, H.-S. (2019). Shape- and size-tunable synthesis of tin sulfide thin films for energy applications by electrodeposition. Applied Surface Science, 479, 167–176. https://doi.org/10.1016/j.apsusc.2019.02.056
5. Rajput, N. (2015). Methods Of Preparation of Nanoparticles – A Review. International Journal of Advances in Engineering & Technology, 7(4), 1806–1811. https://doi.org/10.1016/j.jare.2015.02.007
6. Bragg, W. H., & Bragg, W. L. (1918). X Rays and Crystal Structure. G. Bell and Sons, LTD.
7. P. Scherrer. (1918). Göttinger Nachrichten Gesell. Universität Zu Göttingen, 2, 98.
8. D. Raha, & Das, D. (2013). Nanocrystalline silicon thin films prepared by low pressure planar inductively coupled plasma. J. Appl.Surf. Sci., 276, 249–257.
9. Higler, R., & Sprakel, J. (2017). Doping colloidal bcc crystals — interstitial solids and meta-stable clusters. Scientific Reports, 7(1), 12634. https://doi.org/10.1038/s41598-017-12730-8.
10. Sebastian, S., Kulandaisamy, I., Arulanantham, A. M. S., Valanarasu, S., Kathalingam, A., Shkir, M., & AlFaify, S. (2022). Enhancement in photovoltaic properties of Nd:SnS films prepared by low-cost NSP method. Rare Metals, 41(5), 1661–1670. https://doi.org/10.1007/s12598-019-01295-2.
11. Huang, Z., Thomson, P., & Di, S. (2007). Lattice contractions of a nanoparticle due to the surface tension: A model of elasticity. Journal of Physics and Chemistry of Solids, 68(4), 530–535. https://doi.org/10.1016/j.jpcs.2007.01.016.
12. Aksay, S., Özer, T., & Zor, M. (2009). Vibrational and X-ray diffraction spectra of SnS film deposited by chemical bath deposition method. The European Physical Journal Applied Physics, 47(3), 30502. https://doi.org/10.1051/epjap/2009101.
13. Toda, Y., Hirayama, H., Kuganathan, N., Torrisi, A., Sushko, P. V., & Hosono, H. (2013). Activation and splitting of carbon dioxide on the surface of an inorganic electride material. Nature Communications, 4(1), 2378. https://doi.org/10.1038/ncomms3378.
14. Kihal, R., Rahal, H., Affoune, A. M., & Ghers, M. (2017). Electrodeposition of SnS Thin film Solar Cells in the Presence of Sodium Citrate. Journal of Electrochemical Science and Technology, 8(3), 206–214. https://doi.org/10.33961/JECST.2017.8.3.206.
15. Umar, A., Akhtar, M. S., Badran, R. I., Abaker, M., Kim, S. H., Al-Hajry, A., & Baskoutas, S. (2013). Electrical properties of solution processed p-SnS nanosheets/n-TiO 2 heterojunction assembly. Applied Physics Letters, 103(10), 101602. https://doi.org/10.1063/1.4819838.
16. Srivind, J., Balamurugan, S., Usharani, K., Prabha, D., Suganya, M., Nagarethinam, V. S., & Balu, A. R. (2018). Visible light irradiated photocatalytic and magnetic properties of Fe-doped SnS2 nanopowders. Journal of Materials Science: Materials in Electronics, 29(11), 9016–9024. https://doi.org/10.1007/s10854-018-8926-2.
17. Jose, J., Ravindran, A., & Nair, K. K. (2017). A Review on ZnO Heterojunction Photodetector For UV Application. ICTACT JOURNAL ON MICROELECTRONICS, 2(4), 305–310. https://doi.org/10.21917/ijme.201.
18. Gao, S., Li, W., Dai, J., Wang, Q., & Suo, Z. (2021). ffect of transition metals doping on electronic structure and optical properties of β-Ga 2 O 3. Materials Research Express, 8(2), 025904. https://doi.org/10.1088/2053-1591/abde10.
19. Baco, S., Chik, A., & Md. Yassin, F. (2012). Study on Optical Properties of Tin Oxide Thin Film at Different Annealing Temperature. J. Sci. Technol., 4, 61–72. http://penerbit.uthm.edu.my/ojs/index.php/JST/article/view/468.
20. Dar, M. A., Govindarajan, D., & Dar, G. N. (2021). Facile synthesis of SnS nanostructures with different morphologies for supercapacitor and dye-sensitized solar cell applications. Journal of Materials Science: Materials in Electronics, 32(15), 20394–20409. https://doi.org/10.1007/s10854-021-06550-w.
21. Norton, K., Kunstmann, J., Ping, L., Rakowski, A., Wang, C., Marsden, A. J., Murtaza, G., Zeng, N., McAdams, S. J., Bissett, M. A., Haigh, S. J., Derby, B., Seifert, G., & Lewis, D. J. (2019). Synthetic 2-D lead tin sulfide nanosheets with tuneable optoelectronic properties from a potentially scalable reaction pathway. Chemical Science, 10(4), 1035–1045. https://doi.org/10.1039/C8SC04018D.